Drying layer near a weakly attractive surface

Alla Oleinikova, Ivan Brovchenko and Alfons Geiger

Physical Chemistry, University of Dortmund, 44221 Dortmund, Germany

E-mail: alla@pc2a.chemie.uni-dortmund.de, brov@heineken.chemie.uni-dortmund.de and
alfons.geiger@udo.edu

Abstract
Depletion of the liquid density near a solid surface with a weak long-range
fluid–surface interaction was studied by computer simulations of the liquid–
vapour coexistence of a Lennard-Jones (LJ) fluid confined in slitlike pores.
In a wide temperature range the liquid density decreases towards the surface
without the formation of a *vapour* layer between the liquid and the solid
surface. This evidences the absence of a drying transition up to the liquid–
vapour critical point. Two contributions to the excess desorption Γ_{tot} were
found. The first one, $\Gamma_\xi \sim \rho_{bulk}\xi$, exists at any temperature and diverges
as the bulk correlation length ξ when approaching the liquid–vapour critical
temperature T_c. The second contribution, $\Gamma_L \sim \rho_{bulk}L_0$, originates from a
microscopic *drying layer* near the solid boundary. At high temperatures the
thickness L_0 of the drying layer increases in accordance with the power law
$L_0 \sim -\ln(1 - T/T_c)$, indicating a drying transition at T_c. The *drying layer*
can be suppressed by strengthening the fluid–surface interaction, by increasing
the fluid–surface interaction range or by decreasing the pore size.

1. Introduction

Knowledge of the liquid density profiles near weakly attractive surfaces is necessary for
the understanding of various phenomena, such as hydrophobic attraction between extended
surfaces in water [1], slipping flow of liquids near a weakly attractive surface [2], and
conformational stability of biomolecules in aqueous solutions. Experimental studies evidence
a depletion of the liquid density near weakly attractive substrates [3–8]. However, the shape
of the liquid density profiles could not be derived unambiguously from experimental data.

In the vast majority of practically important situations, the liquid is close to equilibrium
with the vapour, i.e. close to the liquid–vapour coexistence. At the liquid–vapour coexistence
curve the vapour (liquid) phase undergoes a wetting (drying) transition near the solid boundary
at some temperature T_w (T_d) [9–12]. Such a surface transition appears as the formation of
a macroscopically thick liquid layer in the vapour phase near a strongly attractive surface

(wetting transition) or as a vapour layer in the liquid phase near a weakly attractive surface (drying transition). When crossing T_w (T_d) along the liquid–vapour coexistence curve, the liquid (vapour) layer could appear continuously (second-order or critical wetting/drying) or discontinuously (first-order wetting/drying).

Wetting transitions have been extensively studied theoretically, experimentally and by computer simulations for various systems. The temperature of the wetting transition and its order were found to be strongly sensitive to the details of the fluid–fluid and fluid–surface interaction [12]. In particular, in model systems with short-range fluid–surface potential, the wetting transition can be of first or second order, depending on the strength of the fluid–surface potential [10, 13, 14]. The long-range fluid–surface interaction can change drastically the character and temperature of the wetting transition. Critical wetting transitions become first order due to long-range fluid–surface interactions [15]. The interplay between the short-range and long-range fluid–surface interaction potentials can suppress critical wetting up to the liquid–vapour critical temperature [16] and produce a sequential (multiple) wetting transition [17].

A drying transition which is accompanied by the formation of a liquid–vapour interface at some distance from the substrate was observed for short-range fluid–wall interactions (hard-wall [18–20], square-well [14, 21] and truncated LJ interactions [22]) in computer simulations and in density functional studies. Contradictory reports concerning the order of the drying transition in systems with short-range fluid–wall interaction were discussed in [23]. A long-range fluid–surface potential (for example, via van der Waals forces) suppresses a drying transition at subcritical temperatures, which then can occur at the bulk critical temperature T_c only [15, 16, 24]. Since a long-range interaction between fluids and solids is unavoidable in real systems, the formation of a macroscopic vapour layer between the liquid and the surface is impossible. Indeed, a drying transition was never observed experimentally [3, 25].

Although a macroscopic vapour layer cannot appear near a surface with weak long-range attractive potential, an effect distantly related to a drying transition could be expected in the liquid phase below T_c as the appearance of a *drying layer* near the surface (which is not a macroscopic vapour layer and could be considered as 'embryo of drying' [26]). This drying layer can noticeably influence the liquid density profile near a solid surface.

Due to the necessary boundary conditions the behaviour of the fluid density near a planar solid substrate can only be studied by computer simulations in a pore geometry. Most of the computer simulation studies of wetting and drying transitions were performed in NVT ensembles, where slitlike pores with symmetrical or asymmetrical walls were incompletely filled (see, for example, [22, 24]). In such simulations the average density of the confined fluid is deeply inside the two-phase region and a correct reproduction of the liquid–vapour coexistence is questionable. Even when the liquid–vapour interface in such a pore is well established, it is formed parallel to the wall and, therefore, the wetting phase is represented in such a system as a wetting layer only. In our computer simulation studies of surface transitions we use another approach: simulations of the liquid–vapour coexistence curve of fluids, confined in pores of various sizes, with subsequent extrapolation of the results to semi-infinite systems.

The chemical potential of the liquid–vapour phase transition of the confined fluid is shifted with respect to the bulk. This suppresses the formation of a wetting or liquid layer along the liquid–vapour coexistence of the confined fluid below and above the temperature of the wetting transition, respectively [12]. To study the possible appearance of a drying (or vapour) layer in the saturated liquid near a weakly attractive surface, we have investigated the temperature evolution of the density profiles along the pore coexistence curve. The data obtained for fluids in pores of various sizes and with different fluid–surface potentials are compared with the available theoretical predictions and experimental observations.

An LJ fluid was confined in pores of width $H = 40\sigma$ (σ is the molecular diameter) with weakly attractive walls, which interact with the molecules of the fluid via a long-range potential. The well depth of the fluid–surface potential was about 70% of the well depth of the fluid–fluid potential. This is close to the interaction between neon atoms and a caesium substrate, the weakest known physisorption system, recently studied experimentally and by simulations [3, 25]. In our recent paper [27], the liquid–vapour coexistence curve of an LJ fluid was simulated in a smaller pore with $H = 12\sigma$) with the same fluid–surface potential. A depletion of the liquid density near the pore wall was observed in a wide temperature range along the pore coexistence curve without any trend towards the formation of a vapour or drying layer. It was found that the fluid near the wall follows the universal power laws of the surface critical behaviour of Ising systems [28, 29]. In particular, a universal behaviour of the local order parameter profiles, defined as the difference between the local densities $\rho_l(\Delta z, \tau)$ and $\rho_v(\Delta z, \tau)$ of the coexisting liquid and vapour phases at some distance Δz from the pore walls, was observed in a wide temperature range [27, 30, 31]. The intrusion of the surface critical behaviour into the bulk fluid is governed by the bulk correlation length ξ_-, which diverges when approaching the critical point:

$$\xi_-(\tau) = \xi_0 \tau^{-\nu} \tag{1}$$

where $\tau = (1 - T/T_c)$ is the reduced deviation of the temperature T from the bulk critical temperature T_c, $\nu = 0.63$ [32] is the universal critical exponent and ξ_0 is the system-dependent amplitude.

In view of the high sensitivity of the surface phase transitions to small changes of the chemical potential, the observation of a vapour or drying layer in a pore with $H = 12\sigma$ was, probably, prevented by the shift of the liquid–vapour phase transition in such a rather small pore. To reduce the influence of confinement and to promote the observation of a vapour or drying layer, the pore width should be as large as possible. In the present paper we approach the bulk coexistence by performing simulations in a very large pore of width $H = 40\sigma$. To extrapolate the results to a semi-infinite system the liquid–vapour coexistence of the LJ fluid in several pores of intermediate sizes between $H = 12$ and 40σ was simulated.

2. Method

Coexistence curves of the confined LJ fluid were determined using Monte Carlo simulations in the Gibbs ensemble (GEMC) [33]. GEMC simulations allow one to achieve direct equilibration of the two coexisting phases, which are simulated at a given temperature simultaneously in two simulation cells. Equality of the chemical potentials in the two phases is achieved by molecular transfers between the simulation boxes. The efficiency of the molecular transfers was improved by early rejection of insertion attempts with at least one intermolecular distance less than 0.5σ, that would lead to strong repulsion. The acceptance probability of molecular transfers varied from 0.5% at low temperatures to about 10% at high temperatures. Equality of the pressures in the coexisting phases is achieved by random changes of the volumes of the simulation boxes, keeping the total volume of the two boxes constant. The maximal variation of the volume of each box was about 1–1.5%, providing an acceptance probability of this move from 20 to 30%. In the course of the GEMC simulations with overall lengths of 10^8 MC steps, the sequence of MC moves was random. Conventional MC moves, molecular transfers and volume changes were performed with the probabilities ~75%, ~25% and <1%, respectively. For each temperature point the number of successful transfers per particle between the coexisting phases varied from dozens at low temperatures to ~350 near the pore critical temperature. More details of the simulations, parameters of the model fluid, as well as its bulk coexistence curve are given in our previous paper [27].

To study the behaviour of the liquid near the surface, the LJ fluid was confined in a slitlike pore with structureless walls. Each wall interacts with the particles of the fluid via the long-range potential of a single plane of LJ molecules:

$$U_{\text{w}}(z) = 4\epsilon f \left[0.4 \left(\sigma/z \right)^{10} - \left(\sigma/z \right)^4 \right], \tag{2}$$

where z measures the distance to the wall, the parameter f determines the strength of the fluid–wall interaction relatively to fluid–fluid interaction and σ is the diameter of the LJ particles. No truncation was applied to $U_{\text{w}}(z)$. In the present paper we report the results obtained for a pore of width $H = 40\sigma$ and $U_{\text{w1}}(z) = U_{\text{w}}(z, f = 0.3)$, which corresponds to a weakly attractive (solvophobic) surface with a well depth of the fluid–wall interaction of about 70% of the well depth of the fluid–fluid interaction. The total number of molecules in the liquid and vapour phases was about 8000. The average lateral size of the simulation box which contains the liquid phase increases from 17 to 21σ with increasing temperature. To study the effect of the pore size on the liquid density profile and the appearance of a drying layer, we also simulated the liquid–vapour coexistence and the liquid density profiles at $T = 1.10$ in pores of width $H = 16, 22$ and 26σ with the same fluid–wall interaction $U_{\text{w1}}(z)$.

To explore the effect of the strength of the fluid–wall potential on the liquid density profile we also simulated the liquid–vapour coexistence in a pore with slightly stronger fluid–surface interaction $U_{\text{w2}}(z) = U_{\text{w}}(z, f = 0.4)$. Additionally, the effect of the range of the fluid–wall interaction was explored by simulation of a system with a slower decay of the fluid–wall potential $U_{\text{w3}}(z)$, which follows from an integration of the individual interactions over the half-space of LJ molecules and can be described by the equation

$$U_{\text{w3}}(z) = 4\epsilon f^* \left[\left(\sigma^*/z \right)^9 - \left(\sigma^*/z \right)^3 \right]. \tag{3}$$

The parameters of the potential $U_{\text{w3}}(z)$ were adjusted to get equal well depths of the potentials $U_{\text{w3}}(z)$ and $U_{\text{w1}}(z)$. This was achieved using $\sigma^* = 0.8328\sigma$ and $f^* = 0.468$ in equation (3).

The density ρ used in the present paper is the reduced number density (scaled by σ^3), while T is the reduced temperature (scaled by ϵ/k_{B}, where k_{B} is Boltzmann's constant). The average density of the LJ fluid confined in a pore was calculated taking into account the volume accessible to the fluid molecules. The fluid–wall interaction is equal to zero at the distance 0.86σ from the pore wall and so in an operational approach this interval could be divided equally between the volumes of the fluid and the solid. As a result, the volume accessible to the fluid molecules is the total pore volume L^2H reduced by a factor 1.022 for the pore of width $H = 40\sigma$. Accordingly, as the distance to the pore wall Δz we used the distance to the parallel plane 0.5σ inside the pore.

The density profiles of the liquid were obtained by Monte Carlo (MC) simulations in the NVT ensemble, using the average densities of the liquid phase obtained in the GEMC simulations. At high temperatures, the strong density gradient near the pore wall makes the determination of reliable density profiles in such large pores very time consuming. This problem was overcome by using two kinds of move in MC simulations in the NVT ensemble. The first kind of move is a standard MC move with a maximal displacement of molecule, which provides an acceptance probability of about 50%. The second kind of move is a long-distance molecular transfer inside the simulation box: an attempt to place a randomly chosen fluid molecule into a randomly chosen position. This move is similar to the one used in GEMC simulations for molecular transfers between the two simulation boxes. Such long-distance molecular transfers essentially improve the sampling of density profiles, which show a strong gradient normal to the pore wall. The local density was determined for layers of 0.02σ width. The resulting density profiles were averaged over 10^5 configurations taken each 1000th MC step. This yielded a statistical uncertainty less than 1%.
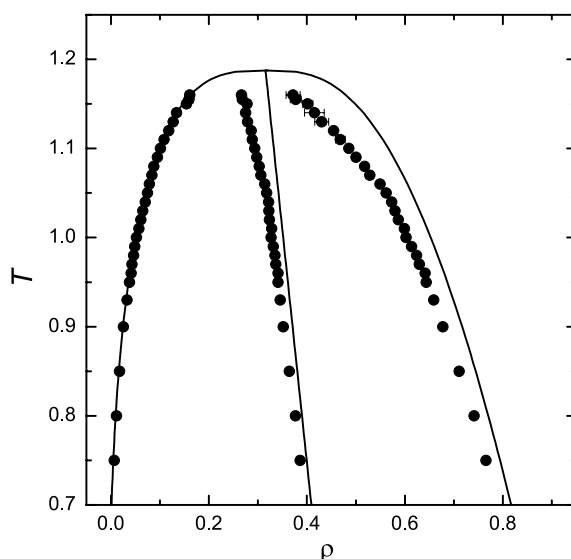
Figure 1. Coexistence curve and diameter of the LJ fluid confined in the slitlike pore of width $H = 40\sigma$ (circles). The bulk coexistence curve (coexisting densities ρ_l and ρ_v) and its diameter $((\rho_l + \rho_v)/2)$ of the LJ fluid [27] are shown by solid lines.

3. Results

The obtained densities of the coexisting vapour (ρ_v) and liquid (ρ_l) phases and the diameter ($(\rho_l + \rho_v)/2$) of the coexistence curve of the LJ fluid in the slitlike pore with weakly attractive walls of width $H = 40\sigma$ are shown in figure 1. The critical temperature of the pore coexistence curve is depressed due to the effect of the confinement. It is estimated as $T = 1.165 \pm 0.005$, that is only about 0.02 below the bulk critical temperature $T_c = 1.1876$ [27, 34]. This indicates that in this case the pore coexistence curve is rather close to the coexistence curve of the bulk fluid. In such a wide pore, we may therefore expect that below the pore critical temperature the properties of the fluid near a wall are only slightly influenced by the presence of the opposite wall.

Figure 1 shows that the average density of the liquid phase at the pore coexistence curve is noticeably lower than the density of the bulk LJ fluid at the same temperature. This effect becomes more pronounced at higher temperatures, i.e., at about $T > 1.05$, and it originates from the depletion of the liquid density near a weakly attractive wall [27, 30, 31, 35, 36]. Indeed, a pronounced decrease of the liquid density near the wall is observed in the large ($H = 40\sigma$) as well as in the small ($H = 12\sigma$ [27]) pore (see figure 2). At high temperatures the liquid density profile is flat in the pore interior (constant $\rho_l(\Delta z, \tau)$ in the central part of the pore) and gradually decreases toward the pore wall, displaying only a single small oscillation near the pore wall (figure 2, upper panel). Upon cooling, the region of density depletion shrinks and additional density oscillations develop gradually on the density profiles. A qualitatively similar behaviour of the density profile is seen in the liquid phase in the small pore of width $H = 12\sigma$ (figure 2, lower panel). In the small pore, however, the density depletion spreads over the whole pore near the pore critical temperature and the flat part of the liquid density profile is not observed.

A direct comparison of the density profiles of the saturated liquid in the small and large pores is shown in figure 3 for some temperatures. At $T = 0.80$ the profiles are practically
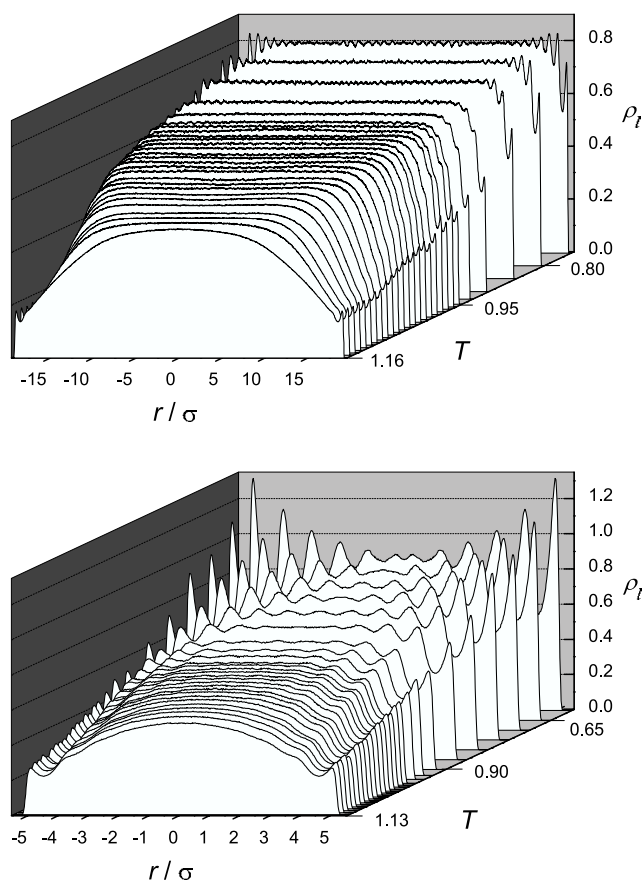
Figure 2. Temperature evolution of the liquid density profile along the pore coexistence curves of the LJ fluid confined in a slitlike pore with $H = 40\sigma$ (upper panel) and $H = 12\sigma$ (lower panel).

identical in both pores. The density oscillations are slightly larger in the small pore. At high temperatures, the density depletion is weaker in the small pore and the difference between $\rho_l(\Delta z, \tau)$ in the small and the large pore becomes more pronounced with increasing temperature.

It was shown [27, 31] that the local order parameter profiles $\Delta\rho(\Delta z, \tau) = (\rho_l(\Delta z, \tau) - \rho_v(\Delta z, \tau))/2$, in the small pore of width $H = 12\sigma$ with weakly attractive walls, collapse into a single master curve when the local order parameter is normalized by the bulk order parameter, and the distance to the pore wall is normalized by the bulk correlation length (see figure 9 in [27]). Such a universal behaviour of $\Delta\rho(\Delta z, \tau)$ evidences that the drying transition, which is expected at the bulk critical temperature, does not influence the liquid density profiles in such a small pore. In the large pore of width $H = 40\sigma$, we do not obtain such universal behaviour of $\Delta\rho(\Delta z, \tau)$ when using the same approach, as described above [27]. We have found that this discrepancy originates from the quite different temperature dependences of the density profiles of the *liquid* phase in small and large pores.

The liquid density profiles at various temperatures can be compared, using the normalized density $\rho_l(\Delta z, \tau)/\rho_{l,bulk}(\tau)$, where $\rho_{l,bulk}(\tau)$ is the liquid density of the bulk LJ fluid (the values, obtained in [27], are shown in the last column of table 1). Because the intrusion of the surface perturbation into the bulk fluid is governed by the bulk correlation length ξ, it
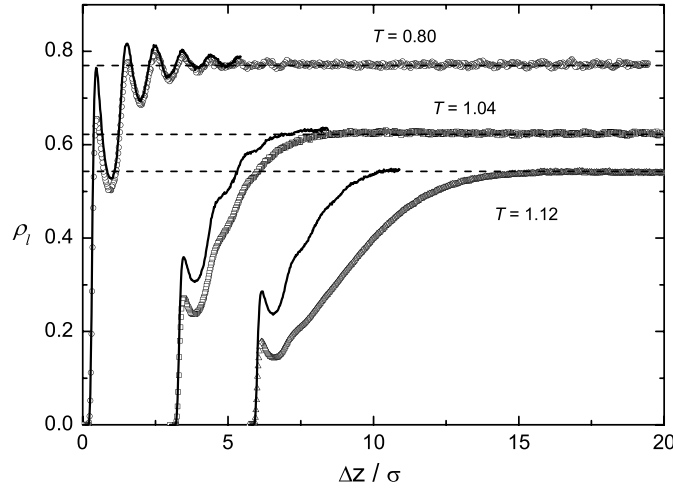
Figure 3. The density profiles of the coexisting liquid phase of the LJ fluids confined in the slitlike pores with $H = 40\sigma$ (symbols) and 12σ (solid lines). The profiles for $T = 1.04$ and 1.12 are shifted to larger Δz by 3 and 6σ, respectively.

is reasonable to display the distance to the pore wall in terms of ξ. Taking into account the universal temperature dependence of ξ along the coexistence curve (equation (1)), we can use $\Delta z/\tau^{-\nu}$ as a normalized distance variable. The normalized density profiles of the liquid in the small and the large pore are compared in figure 4 in the temperature range from $T = 1.04$ up to the highest temperature of the two-phase coexistence in the pore.

In the small pore, the normalized density profile $\rho_l(\Delta z, \tau)$ can be roughly described by the exponential equation

$$\frac{\rho_l(\Delta z, \tau)}{\rho_{l,bulk}(\tau)} = \left[1 - \exp\left(-\frac{\Delta z - l_0}{\xi_0 \tau^{-\nu}} \right) \right]. \tag{4}$$

The values of the parameter l_0 obtained from the fits do not exceed a few tenths of σ, whereas the value of the fitting parameter ξ_0 is about 0.3σ, close to the value of ξ_0 obtained from the master curve of the order parameter profiles in [27]. In the large pore, the shape of the liquid density profiles is qualitatively different from that in the small pore (figure 4). Moreover, in the large pore the normalized profiles $\rho_l(\Delta z, \tau)/\rho_{l,bulk}(\tau)$ vary with temperature non-monotonically with the 'lowest' profile at $T = 1.11$ (see figure 4). The shape of the liquid density profiles at any temperature cannot be fitted to the exponential equation (4).

These peculiarities of the liquid density profiles in the large pore indicate the possible presence of some non-universal contribution to the surface behaviour. As the increase of the pore size can be considered as an approach to a semi-infinite system, one may expect that this peculiar behaviour is connected with the formation of a drying layer, caused by a drying transition at the bulk critical temperature [12]. If such a drying layer appears in a liquid phase near the surface of a large pore, the liquid density profile should be described by an interface-like equation. The density profile at the intrinsic liquid–vapour interface, derived from the van der Waals theory, could be described by the following equation [37, 38]:

$$\rho_l(\Delta z, \tau) = \frac{\rho_{l,bulk}(\tau) - \rho_{v,bulk}(\tau)}{2} \tanh\left(\frac{\Delta z - L_0}{2\xi_-} \right) + \frac{\rho_{l,bulk}(\tau) + \rho_{v,bulk}(\tau)}{2}, \tag{5}$$

where L_0 is the distance from the liquid–vapour interface to the solid surface. This intrinsic interfacial profile can be affected by capillary waves, i.e., thermal fluctuations of
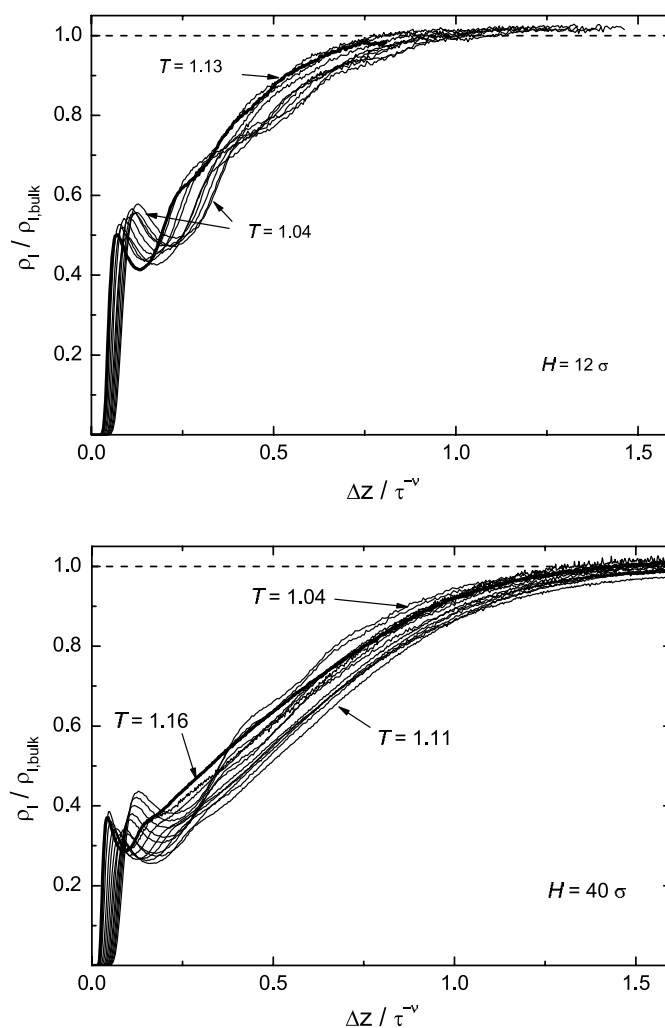
Figure 4. Scaling plot for the liquid density profiles in the small pore with $H = 12\sigma$ for $T = 1.04$, 1.05, 1.06, 1.07, 1.08, 1.09, 1.10, 1.11, 1.12 and 1.13 (upper panel) and in the large pore with $H = 40\sigma$ for $T = 1.04$, 1.05, 1.06, 1.07, 1.08, 1.09, 1.10, 1.11, 1.12, 1.13, 1.14, 1.15, 1.155 and 1.16 (lower panel). The highest studied temperature for each pore is shown by a thick solid line.

the interface [39]. Far from the critical point the bulk fluctuations are small and capillary waves are the dominant factor, which determines the thickness of the interface [40]. Upon increasing the temperature the density fluctuations in the bulk phases become more important, yielding an intrinsic interfacial thickness proportional to the increasing bulk correlation length, as described by equation (5). Since the expected interface is close to the wall, the capillary waves can be suppressed by a long-range fluid–surface interaction.

We have found that the liquid density profile in the large pore can be described by equation (5) at low temperatures, when the density of the bulk vapour is close to zero. However, equation (5) fails to fit the liquid density profiles at high temperatures, because the value of the density near the pore wall is even lower than the bulk vapour density at the same temperature. This result is consistent with the theoretical expectations that a vapour layer never appears

Table 1. The values of the fitting parameters ξ_-, L_0 and $\rho_{l,bulk}$ in equation (6) when fitted to the liquid density profiles in the large pore of width $H = 40\sigma$ at different temperatures T (reduced temperatures τ). Uncertainties of the fitting parameters correspond to the confidence level 95%. The values of $\rho_{l,bulk}^0$ were obtained by direct GEMC simulations of the liquid–vapour equilibrium [27].

T	τ	ξ_-/σ ± 0.01	L_0/σ ± 0.01	$\rho_{l,bulk}$ ± 0.0005	$\rho_{l,bulk}^0$
0.75	0.368	0.19	0.92	0.7935	0.793
0.80	0.326	0.24	0.89	0.7703	0.769
0.85	0.284	0.35	0.83	0.7424	0.743
0.90	0.242	0.56	0.84	0.7161	0.717
0.93	0.217	0.62	0.89	0.6996	0.697
0.95	0.200	0.69	0.99	0.6880	0.684
0.96	0.192	0.66	0.92	0.6826	0.678
0.97	0.183	0.75	1.05	0.6764	0.672
0.98	0.175	0.67	0.95	0.6649	0.665
0.99	0.166	0.81	1.14	0.6634	0.659
1.00	0.158	0.87	1.29	0.6560	0.651
1.01	0.150	0.82	1.17	0.6484	0.644
1.02	0.141	0.82	1.23	0.6362	0.637
1.03	0.133	0.89	1.31	0.6328	0.628
1.04	0.124	0.87	1.31	0.6247	0.622
1.05	0.116	0.95	1.40	0.6164	0.613
1.06	0.107	1.10	1.57	0.6103	0.605
1.07	0.099	1.16	1.73	0.5920	0.597
1.08	0.091	1.16	1.84	0.5830	0.590
1.09	0.082	1.31	1.23	0.5760	0.576
1.10	0.074	1.47	2.26	0.5630	0.568
1.11	0.065	1.57	2.69	0.5550	0.558
1.12	0.057	1.68	2.71	0.5420	0.547
1.13	0.049	1.95	2.87	0.5210	0.529
1.14	0.040	2.14	3.18	0.5140	0.524
1.15	0.032	2.40	3.28	0.5036	0.502
1.155	0.027	2.91	3.69	0.5065	0.495
1.16	0.023	3.32	3.75	0.493	0.488

near a surface with long-range fluid–surface interaction [15, 16]. So, it is more reasonable to suggest not a *vapour* but a *drying* layer near the surface. Since the density distribution in a drying layer is unknown, we fitted the liquid density profiles to equation (5) with $\rho_{v,bulk}$ as a free parameter ρ^*. Such an approach provides a satisfactory description of the simulated profiles apart from the first layer of about σ width, where a density oscillation, caused by fluid–surface interaction potential, is noticeable even at supercritical temperatures. The values of ρ^* obtained from the fits were found close to zero for all studied temperatures. An example of such a fit with $\rho^* = 0$ for $T = 1.10$ is shown in figure 5. So, we propose the following equation to describe the liquid density profile $\rho_l(\Delta z, \tau)$ near a weakly attractive surface:

$$\rho_l(\Delta z, \tau) = \frac{\rho_{l,bulk}(\tau)}{2}\left[\tanh\left(\frac{\Delta z - L_0}{2\xi_-}\right) + 1\right]. \tag{6}$$

There are three parameters in equation (6): L_0, the distance of the inflection point of the such defined liquid–drying layer interface from the surface (thickness of the drying layer), ξ_-, the bulk correlation length at the liquid–vapour coexistence curve, and $\rho_{l,bulk}(\tau)$, the density of the bulk liquid. The first density oscillation (which extends over about 1σ near the surface)
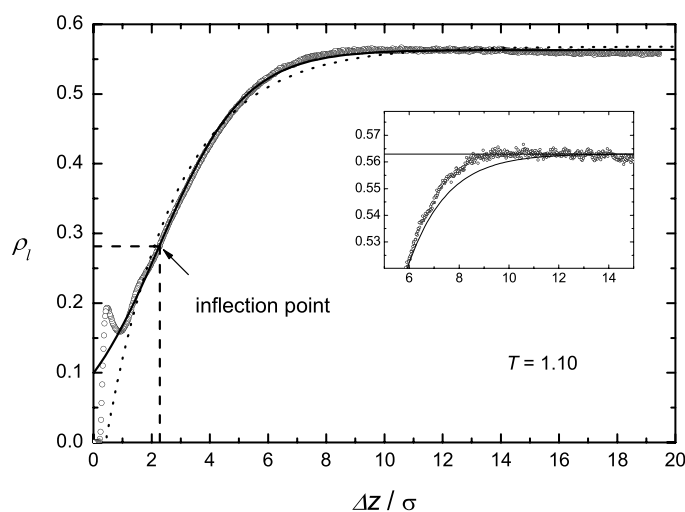
Figure 5. Liquid density profile in the large pore with $H = 40\sigma$ at $T = 1.10$ (circles) and the fit to equation (6) with the parameters shown in table 1 (solid line) and to equation (4) (dotted line). Coordinates of the inflection points are shown by dashed lines. The inset gives a sectoral magnification. The value $\rho_{l,bulk}$ found from the fit is shown by the horizontal line in the inset.

is caused by the localization of the molecules in the well of the fluid–wall potential. Since it strongly deviates from the smooth density profile outside the first layer, it is reasonable to exclude the first layer from the fits. The values of the parameters obtained from the fits of equation (6) to the simulated liquid density profiles are shown in table 1.

The temperature dependences of the correlation length ξ_- and of the thickness of the drying layer L_0, obtained from these fits, are shown in figure 6 (solid circles). The correlation length shows a temperature dependence, which is rather close to the simple power law described by equation (1) with an amplitude $\xi_0 = 0.28\sigma$ (figure 6, lower panel, dashed line). Such an amplitude of the correlation length agrees well with the value $\xi_0 = 0.3\sigma$, obtained previously from the master curve of the order parameter of an LJ fluid in a narrow pore [27].

Another estimate of the amplitude of the correlation length can be obtained based on the exponential decay of the perturbation caused by the surface: far from the surface the deviation of the local density from the bulk value is governed by the bulk correlation length and should follow equation (4). Thus, the progressive exclusion of an increasing part of the density profile near the surface from the fit should show a convergence of the fitting parameters, including ξ_-. The values of ξ_- obtained from fits of equation (4) to liquid density profiles, which extend from the pore centre to various distances from the surface Δz_{cut}, are shown in figure 7 (lower panel) for two temperatures. A clear convergence of the fitted values ξ_- is observed, when the fitted part of the density profile does not approach the pore wall closer than 6σ at $T = 1.15$ and 8σ at $T = 1.16$. These converged values of ξ_- are remarkably close to the values of ξ_- obtained from the fit of the data to equation (6), shown by dashed lines (figure 7).

The values $\rho_{l,bulk}$ obtained from fits of $\rho_l(\Delta z, \tau)$ to the interfacial equation (6) (table 1) are almost equal to the liquid densities in the pore centre, obtained by fits of the data near the pore centre to the exponential equation (4) (see solid lines in figure 7). The values $\rho_{l,bulk}$ obtained from these fits agree very well with the bulk liquid densities obtained by direct Gibbs ensemble MC simulations of the liquid–vapour equilibrium [27], which are also presented in table 1.
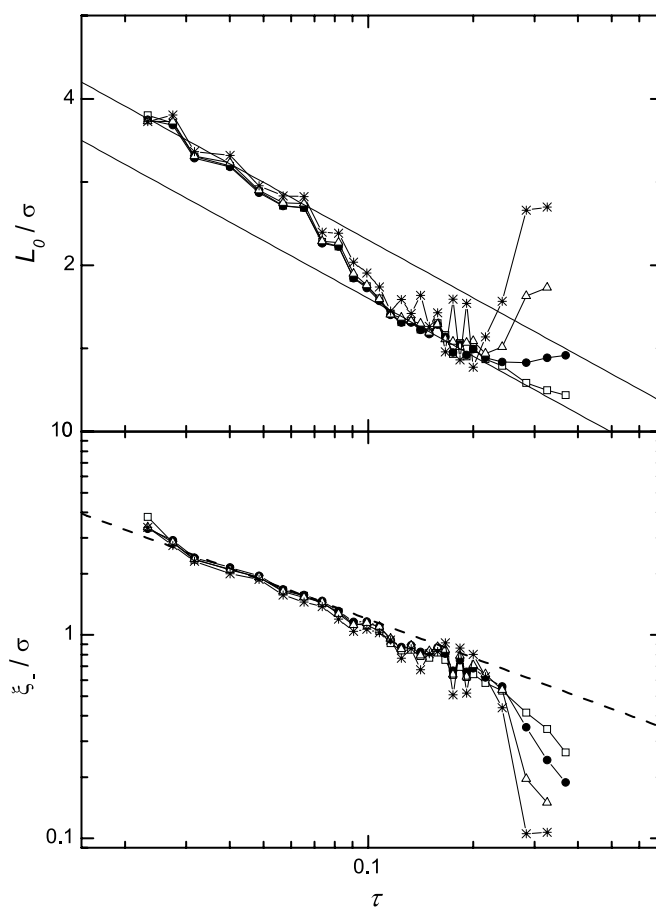
Figure 6. Temperature dependence of the thickness of the drying layer L_0 and correlation length ξ_-, obtained from the fits of equation (6) to the part of the liquid density profile $\rho_l(\Delta z, \tau)$, which extends from the pore centre to various distances Δz_{cut} from the surface: $\Delta z_{cut} = 0\sigma$ (squares), 1σ (circles), 2σ (triangles) and 3σ (stars). A logarithmic behaviour described by equation (7) with const $= -0.05\sigma$ and -0.85σ is shown by upper and lower solid lines, respectively. The power law (1) with $\xi_0 = 0.28\sigma$ is shown by a dashed line.

Next, we test the sensitivity of the fitting parameters in the interfacial equation (6) from the portion of the liquid density profile used for the fits. For this purposes we fitted equation (6) to the part of $\rho_l(\Delta z, \tau)$, which extends from the pore centre to some distances Δz_{cut} from the surface. The fitting parameter $\rho_{l,bulk}$ was found to be practically independent of the choice of the fitting interval. The values of the correlation length ξ_-, obtained from the fits, depend on the choice of Δz_{cut} (from 0 to 3σ) only at $T \leqslant 0.90$ or $\tau \geqslant 0.24$ (see figure 6, lower panel) due to the strong density oscillations near the surface at low temperatures. At $T > 0.90$ the fitting results for the correlation length ξ_- are not sensitive to Δz_{cut}.

The change of the thickness of the drying layer L_0 with temperature is shown in the upper panel of figure 6. At the lowest temperatures ($T \leqslant 0.90$ or $\tau \geqslant 0.24$) the fitted value of L_0 is determined by the choice of Δz_{cut}, namely $L_0 \approx \Delta z_{cut}$. This correlation is clearly imposed by the strong density oscillations near the surface. Thus, if the thickness of a drying layer does not exceed 1σ, meaningful value of L_0 cannot be determined from the fits. At higher
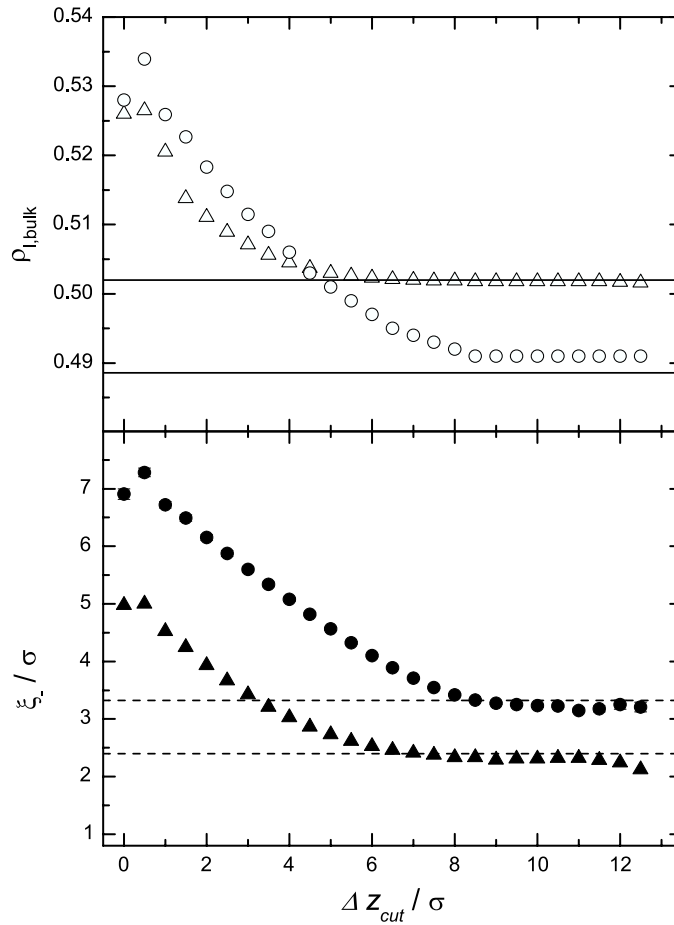
Figure 7. Variation of the fitting parameters $\rho_{l,bulk}$ and ξ_- at $T = 1.15$ (triangles) and $T = 1.16$ (circles), when equation (4) is fitted to those parts of the liquid density profile $\rho_l(\Delta z, \tau)$ which extend from the pore centre to various distances Δz_{cut} from the surface. The values of the liquid density at the bulk coexistence curve are shown by solid lines (upper panel). The values of the bulk correlation length ξ_-, obtained from the fit of equation (6) to $\rho_l(\Delta z, \tau)$ (table 1), are shown by dashed lines (lower panel).

temperatures, L_0 does not depend noticeably on the choice of Δz_{cut}. Two temperature regions could be distinguished in the temperature dependence of L_0 at $T > 0.90$. In the temperature interval from $T = 1.11$ to 1.16 ($0.023 < \tau < 0.065$) the thickness of a drying layer L_0 clearly follows the logarithmic dependence

$$L_0 = \ln(\tau^{-1}) + \text{const} \tag{7}$$

with const $\approx -0.05\sigma$ (see figure 6, upper panel, upper solid line). A quite similar logarithmic temperature dependence of L_0 is observed in the low-temperature interval from $T = 0.85$ to 1.06 ($0.11 < \tau < 0.28$), but with another value const $\approx -0.85\sigma$. There is a crossover between two kinds of logarithmic behaviour in the temperature interval from $T = 1.07$ to 1.10 ($0.074 < \tau < 0.10$). Note that the observed logarithmic temperature dependence of L_0 is similar to that predicted for the divergence of the thickness of the wetting layer in the case of a critical wetting transition [12]. We have also fitted the obtained temperature dependence of
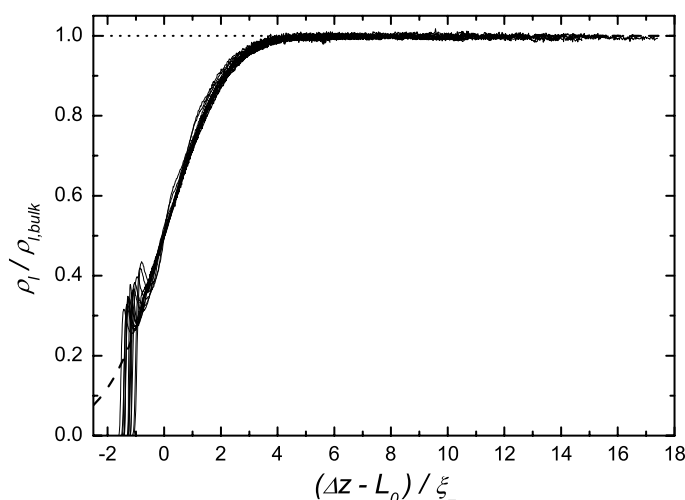
Figure 8. Scaling plot of the liquid density profiles $\rho_l(\Delta z, \tau)$ in the large pore $H = 40\sigma$ for the same temperatures as in figure 4. The parameters $\rho_{l,bulk}$ and L_0 were obtained from fits of equation (6) to density profiles $\rho_l(\Delta z, \tau)$, which were cut at the distance 1.0σ from the surface (table 1). For $T = 1.16$ the value $\rho_{l,bulk}$ from the bulk coexistence curve was used.

L_0 to the power law

$$L_0 \sim \tau^{-x}, \tag{8}$$

as the thickness of a drying (wetting) layer is expected to follow a power-law behaviour in some model cases [12]. The value of the exponent x obtained from the fit of L_0 in the temperature interval $1.11 \leqslant T \leqslant 1.16$ ($0.023 \leqslant \tau \leqslant 0.065$) was found to be close to zero. This also supports a logarithmic divergence of L_0 when approaching the critical temperature.

So, equation (6) allows the description of the liquid density profiles in a wide temperature range using two properties of the bulk fluid ($\rho_{l,bulk}$ and ξ_-) and the thickness of the drying layer L_0. The degree of the universality of the liquid density profiles can be illustrated by a master curve, which is essentially improved in comparison with figure 4, where the presence of a drying layer was neglected. Now, we introduce a normalized length scale, which is measured from the liquid–drying layer interface, as $(\Delta z - L_0)/\xi_-$. Using the fitting parameters L_0 and $\rho_{l,bulk}$ from table 1, the liquid density profiles collapse on a single master curve in a wide temperature range $1.04 < T < T_c$ or $0 < \tau < 0.12$ (see figure 8). The dashed line in figure 8 represents the interfacial equation (6) in normalized coordinates. This means that equation (6) allows a perfect description of the liquid density profiles in the whole temperature range, where the drying layer can be clearly detected. In the temperature range above $T = 1.11$ ($\tau = 0.065$), where the thickness of the drying layer follows equation (7) (see figure 6), $\rho_l(\Delta z, \tau)$ can be predicted if the bulk density, the bulk correlation length and the value of const in equation (7) are known. Note that the latter value can be estimated from a single density profile.

We also test the possibility to describe the density profiles of the liquid in the small pore with $H = 12\sigma$ by the interfacial equation (6). The obtained fitting values of L_0 are about 1σ in the whole temperature range (figure 9). The fitting values of L_0 in the small and large pores coincide at low temperatures ($T < 0.90$ or $\tau > 0.24$), where they are strongly influenced by the density oscillations and, therefore, are meaningless. Insofar as a thickness of the drying layer below 1σ cannot be detected from the fits, the real thickness of the drying layer can be essentially lower. Thus, the fitting values of L_0 for the small pore with $H = 12\sigma$, shown in
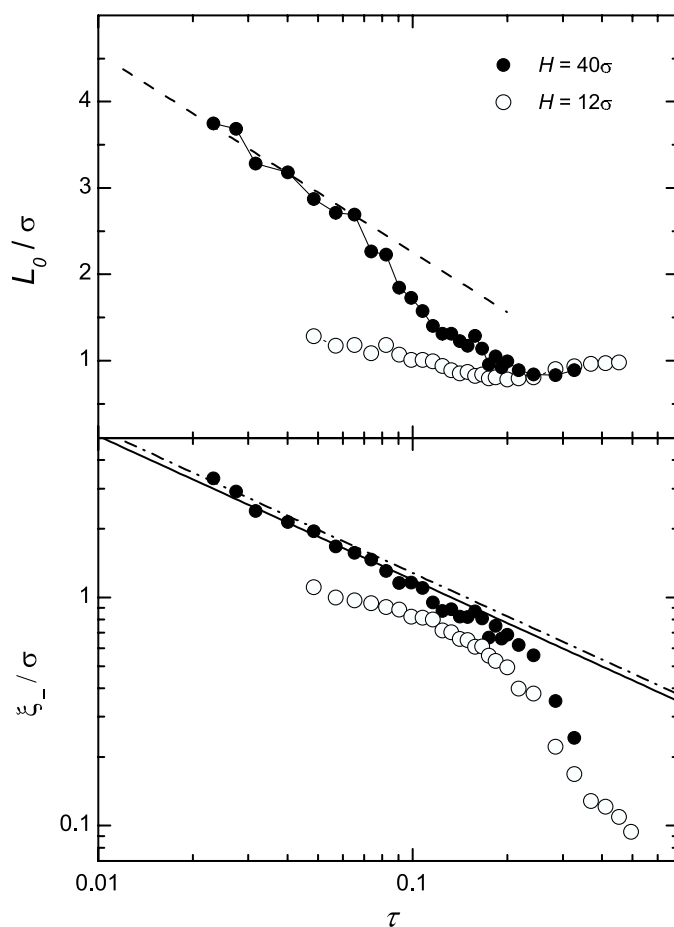
Figure 9. Temperature dependence of the thickness of the drying layer L_0 and of the correlation length ξ_-, obtained from fits of the liquid density profiles $\rho_l(\Delta z, \tau)$ cut at the distance 1σ from the surface for large (solid circles) and small (open circles) pores. The solid and dot–dashed lines represent equation (1) with $\xi_0 = 0.28\sigma$ (this paper) and $\xi_0 = 0.30\sigma$ [27], respectively. The dashed line corresponds to equation (7) with const $= -0.05\sigma$.

figure 9, cannot be considered as an indication of a drying layer in this pore even near the pore critical temperature. Obviously, the fluid layer near the surface, highly localized in the well of a fluid–wall potential, cannot be considered as a drying layer. This observation agrees with a previous analysis of the local order parameter in the same pore [27], which indicated the absence of a drying layer.

The values of ξ_- found from the fits of $\rho_l(\Delta z, \tau)$ in the small pore with equation (6) are noticeably smaller than ξ_- obtained from the fits of the order parameter in the same pore [27] and ξ_- in the large pore (figure 9). So, the liquid density profiles in the small pore cannot be described correctly by equation (6): the effective thickness of the drying layer is ultimately overestimated in such a pore, resulting consequently in an underestimation of the value of the correlation length.

The drying layer, clearly seen in a large pore with $H = 40\sigma$, disappears in a small pore with $H = 12\sigma$ and the same fluid–surface potential. This agrees with the theoretical
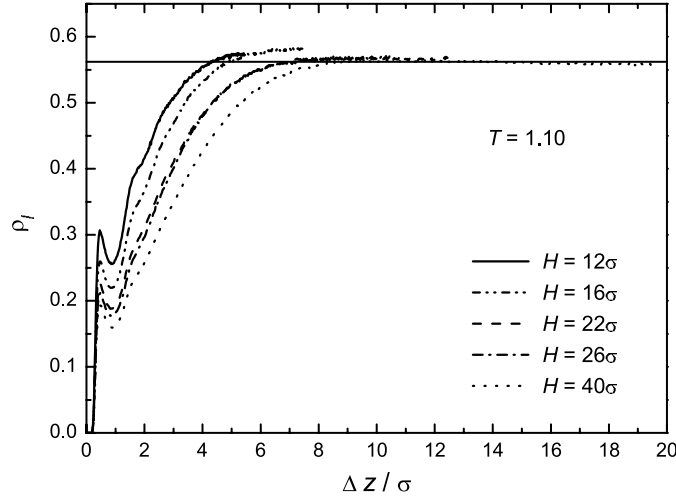
Figure 10. Liquid density profiles $\rho_l\,(\Delta z, \tau)$ at $T = 1.10$ in pores of various width with identical fluid–surface interaction potential, described by equation (2). The liquid density of the bulk fluid is shown by a horizontal line.

expectation of strong sensitivity of the thickness of the drying layer to the chemical potential, which is shifted due to the confinement in the pore [12]. One may expect that the thickness of a drying layer L_0 should continuously increase with increasing pore size and achieve some saturation value $L_{0,\text{inf}}$ in a semi-infinite system. To check this expectation we have simulated liquid–vapour coexistence of the LJ fluid in several pores of various sizes with the same fluid–surface interaction potential at $T = 1.10$. The obtained liquid density profiles shown in figure 10 indicate that the density depletion becomes more pronounced in larger pores. The fits of $\rho_l(\Delta z, \tau)$ with equation (6) allow an estimation of the parameters L_0 and ξ_- in all studied pores, and their dependences on the pore size are presented in figure 11. Note that at this temperature, L_0 exceeds 1σ and the drying layer is indeed detectable in all pores except the smallest one with $H = 12\sigma$. As the shift $\Delta\mu$ of the chemical potential of the phase transition in a pore relatively to a semi-infinite system is proportional to $1/H$ [41], it is reasonable to consider the dependence of L_0 and ξ_- on $1/H$. Both parameters show essentially a linear dependence (see figure 11). Extrapolation of these linear dependences to a semi-infinite system $(1/H \to 0)$ gives the values $L_{0,\text{inf}} = (2.67 \pm 0.15)\sigma$ and $\xi_{-,\text{inf}} = (1.65 \pm 0.04)\sigma$. Assuming that a drying layer effectively decreases the pore size to $H - 2L_0$, the dependences shown in figure 11 become nonlinear and their extrapolation to semi-infinite systems by second-order polynomial fit gives $L_{0,\text{inf}} = (2.79 \pm 0.47)\sigma$ and $\xi_{-,\text{inf}} = (1.73 \pm 0.09)\sigma$. The values of ξ_-, extrapolated to a semi-infinite system, correspond to an amplitude of the correlation length $\xi_0 \approx 0.32$–0.33σ. This value is about 15% higher than the value $\xi_0 = 0.28\sigma$ obtained in the pore with $H = 40\sigma$.

Finally, we have tested the general theoretical expectation that the formation of a drying layer could be suppressed by a strengthening fluid–surface interaction or by extending its attractive range. For this purpose we have simulated liquid–vapour coexistence and density profiles of the coexisting phases in the large pores $(H = 40\sigma)$ at $T = 1.05$, 1.10 and 1.15 with stronger interaction potential $U_{\text{w2}}(z)$ and with the slower decaying potential $U_{\text{w3}}(z)$ (see section 2 for more details). The obtained density profiles at $T = 1.10$ are compared in figure 12. Evidently, the drying layer is strongly influenced by the interaction potential.
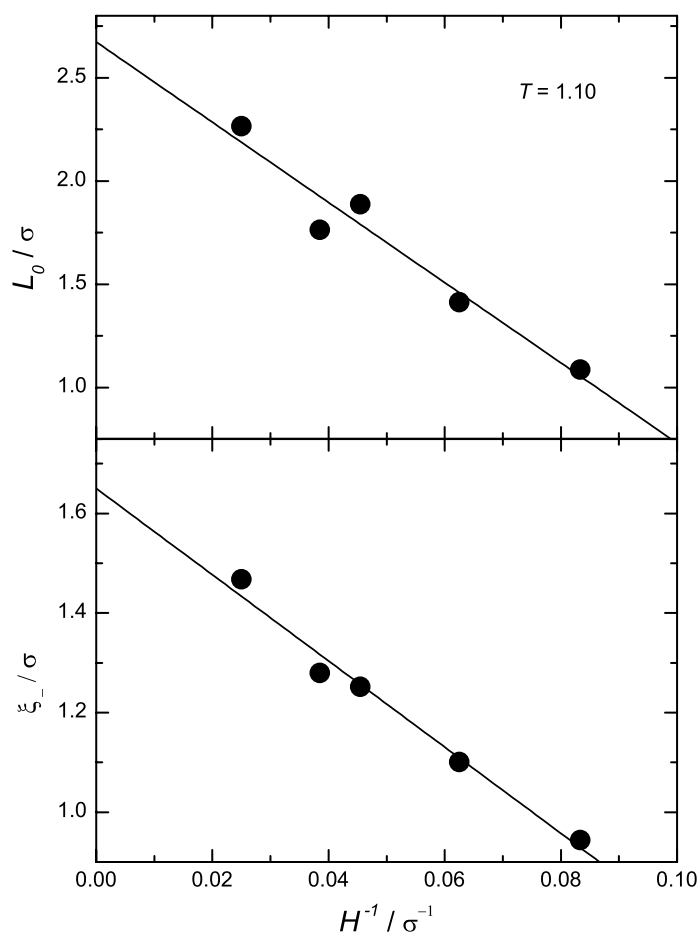
Figure 11. Dependence of the thickness of the drying layer L_0 and the correlation length ξ_-, obtained from fits of the liquid density profile $\rho_l(\Delta z, \tau)$ with equation (6), on the inverse pore width $1/H$ (circles). Linear fits of the data are shown by lines.

Namely, strengthening of the fluid–surface potential by about 33% causes a shrinking of a drying layer at $T = 1.10$ from 2.26σ to 1.76σ, i.e., by about 20%. At $T = 1.05$ the effective thickness of the drying layer is suppressed to about 1σ. An extension of the attractive range of the fluid–surface potential from $\sim r^{-4}$ to $\sim r^{-3}$ has an even stronger effect: the drying layer almost disappears ($L_0 < 1.4\sigma$ at $T = 1.10$).

Starting from the inflection point, the shape of the liquid density profiles remains highly universal for all considered fluid–surface potentials, as it is determined mainly by the bulk correlation length (see lower panel in figure 12). Note that the details of the long-range attractive tail of a fluid–surface potential can produce some minor deviations of $\rho_l(\Delta z, \tau)$ from the universal shape, described by equation (6). An example of such deviations is also shown in the inset of figure 5.

Using the obtained density profiles of the liquid, we analysed the surface excess desorption, which describes a deficit of mass per unit surface area caused by depletion of the liquid density near the surface. The total excess desorption Γ_{tot} contains two contributions: desorption due to the presence of a drying layer Γ_L and desorption due to the density depletion Γ_ξ, governed
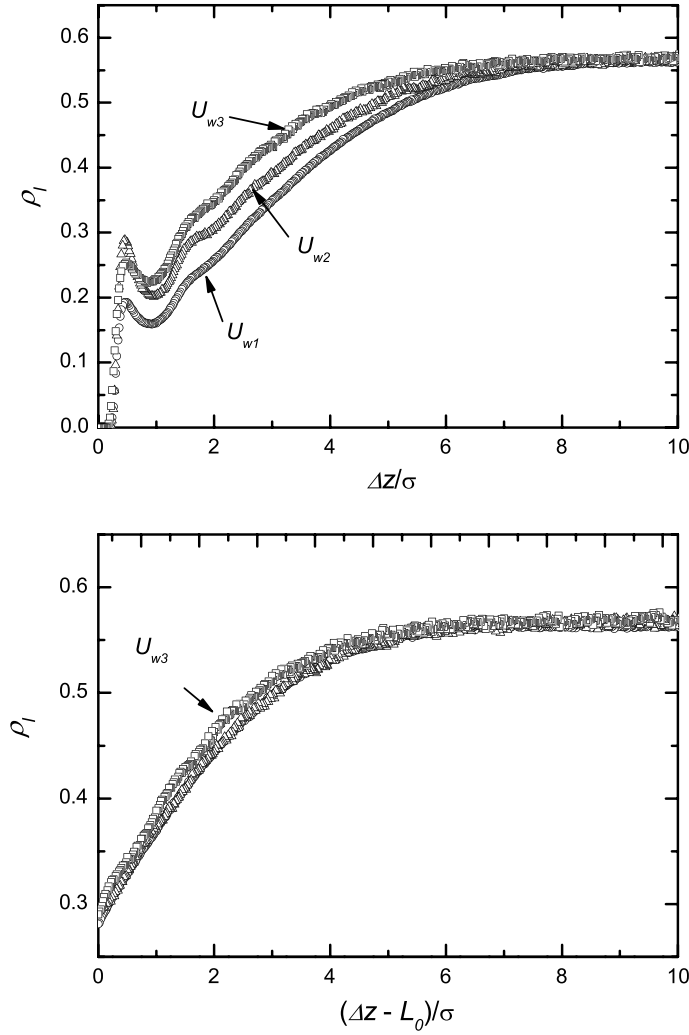
Figure 12. Upper panel: liquid density profiles $\rho_l(\Delta z, \tau)$ at $T = 1.10$ (circles) in pores of width $H = 40\sigma$ with fluid–wall interaction potentials $U_{w1}(z)$ (circles), $U_{w2}(z)$ (triangles) and $U_{w3}(z)$ (squares). Lower panel: the same profiles shown as a function of the distance to the inflection points (see text).

by the correlation length. We calculated these two contributions by numerical integration of $\rho_l(\Delta z, \tau)$ from the surface to the inflection point (Γ_L) and from the inflection point to the pore centre (Γ_ξ). The total excess desorption Γ_{tot} and its two contributions are shown in figure 13 as functions of the reduced temperature. For a semi-infinite system the excess desorption Γ_ξ can be simply calculated by integration of equation (6) for the liquid–drying layer interface from the inflection point to infinity:

$$\Gamma_\xi(\tau) = \rho_{l,\text{bulk}} \xi_- \ln 2. \tag{9}$$

This part of the total desorption behaves like $\sim \tau^{-\nu}$ at any temperature and strongly diverges when approaching the critical point. The contribution Γ_L can be obtained in a similar way, using integration of equation (6) for the liquid–drying layer interface from the pore wall to the
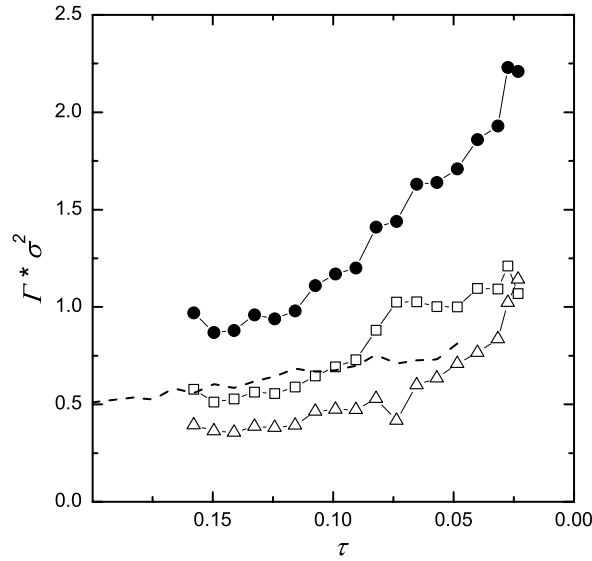
Figure 13. Temperature dependence of the excess desorption of the liquid in the large pore: total excess desorption Γ_{tot} (solid circles) and its contributions due to the drying layer Γ_L (squares) and due to the increase of the correlation length Γ_ξ (triangles). Total desorption in the small pore is shown by dashed line.

inflection point:

$$\Gamma_L(\tau) = \rho_{l,bulk} \left[L_0 + 2\xi_- \ln\left(\cosh(L_0/2\xi_-) \right) \right] / 2. \tag{10}$$

We analysed the ability of equations (9) and (10) to describe the simulation results of the excess desorption. The excess desorption Γ_ξ depends on the bulk fluid properties only. Knowing the temperature behaviour of the bulk liquid density $\rho_{l,bulk}$ along the coexistence curve [27] and using the asymptotic equation (1) for the bulk correlation length with amplitude $\xi_0 = 0.28\sigma$, we can directly obtain the temperature dependence of Γ_ξ from equation (9) (dashed line in figure 14). Good agreement of the simulated values of Γ_ξ with equation (9) is observed in the whole temperature range studied. Deviations at low and high temperatures should be attributed to deviations of the correlation length from the asymptotic equation (1) (see figure 6).

The excess desorption Γ_L, described by equation (10), apart from the bulk parameters $\rho_{l,bulk}$ and ξ_-, contains also the parameter L_0, determined by the fluid–surface interaction. We obtain meaningful estimates of L_0 for the temperatures, where the thickness of the drying layer L_0 exceeds about 1σ. In this range L_0 follows equation (7) (see figure 6) and therefore the contribution Γ_L varies roughly as $\ln (\tau^{-1})(\rho_{l,bulk})/2$, i.e., shows logarithmic divergence when approaching T_c. The excess desorption Γ_L described by equation (10), and the total excess desorption $\Gamma_{tot} = \Gamma_\xi + \Gamma_L$, described by equations (9) and (10), are shown in figure 14 by dashed–dot and solid lines, respectively. Obviously, good agreement of the simulated values of Γ_L with equation (10) is observed in the range where the temperature dependence of L_0 is known.

In a wide temperature range the contribution from the drying layer to the excess desorption is dominant (figure 13). However, the contributions Γ_L and Γ_ξ approach each other with increasing temperature and practically coincide at $\tau \approx 0.02$ (figure 14). The contribution Γ_ξ obviously should dominate Γ_L at higher temperatures, as the former diverges as $\tau^{-\nu}$, whereas the latter diverges logarithmically only.
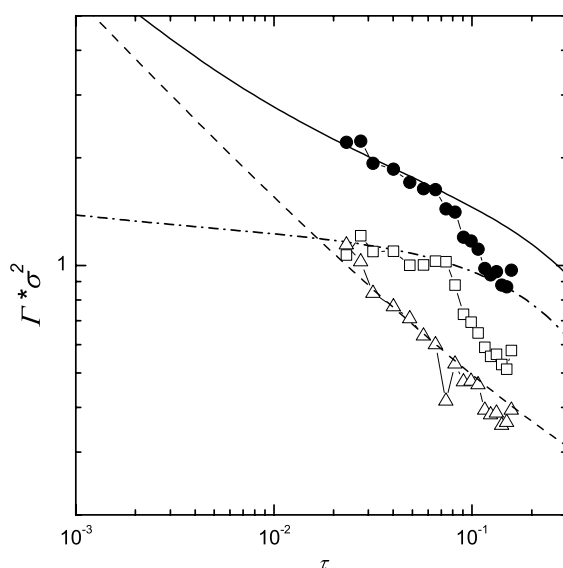
Figure 14. Temperature dependence of the excess desorption of the liquid in double logarithmic scale: the symbols are the same as in figure 13. Desorption Γ_ξ, Γ_L described by equations (9) and (10) and $\Gamma_{tot} = \Gamma_\xi + \Gamma_L$ are shown by dashed, dashed–dot and solid lines, respectively.

4. Discussion

We have studied the temperature evolution of the density profiles of a liquid along the liquid–vapour coexistence curve near a weakly attractive surface. To approach the fluid behaviour in a semi-infinite system, the liquid–vapour coexistence curve of an LJ fluid was simulated in an extremely large slitlike pore with $H = 40\sigma$. Additionally, at some temperatures we simulated the liquid–vapour coexistence in pores of various sizes. Strong depletion of the liquid density near a weakly attractive pore wall is observed. The shape of the liquid density profiles evidences the formation of a drying (not a vapour) layer near the pore wall with increasing temperature. This drying layer can be detected at $T > 1.0$ ($\tau < 0.15$), when the distance between the inflection point of the density profile and the pore wall exceeds at least one molecular diameter. We propose to describe the liquid density profiles near weakly attractive surfaces by equation (6), which assumes an interface between the liquid phase and the drying layer and allows estimation of the bulk correlation length ξ_- and the thickness of the drying layer L_0.

The fits of $\rho_l(\Delta z, \tau)$ with the interfacial-like equation (6) and with the exponential equation (4) which describes the decay to the bulk density far from the surface give similar values of the amplitude of the correlation length $\xi_0 \approx 0.28\sigma$. This evidences a self-consistency of the proposed treatment of the liquid density profile and also indicates a negligible effect of the capillary waves on the studied interface between the liquid and the drying layer. This conclusion corroborates general theoretical arguments, concerning the influence of a long-range fluid–surface potential on the interface between the vapour and the wetting layer [12].

The thickness of the drying layer L_0 follows a logarithmic temperature dependence (7), starting from $T \approx 1.1$ (i.e., at $\tau < 0.074$). Such a logarithmic divergence with approaching wetting (drying) temperature is expected for critical wetting (drying) [12]. This result is consistent with the existence of a second-order drying transition at the bulk critical temperature
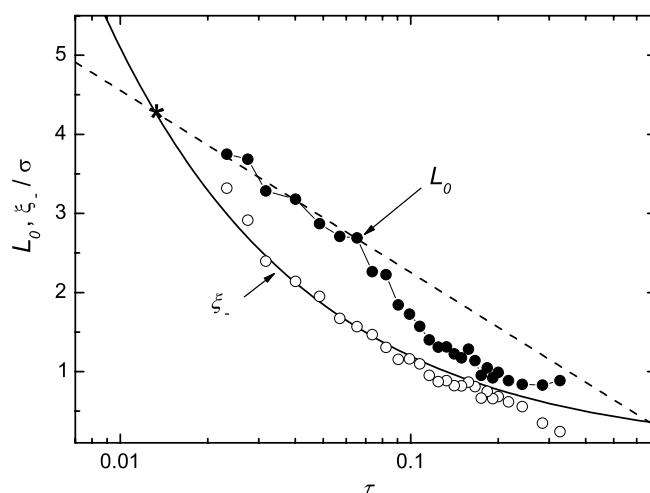
Figure 15. Temperature dependence of the thickness of the drying layer L_0 (solid circles) and correlation length ξ_- (open circles), obtained from fits of the liquid density profile $\rho_l\,(\Delta z, \tau)$, which extend from the pore centre to the distance 1σ from the surface. The logarithmic law described by equation (7) with const $= -0.05\sigma$ is shown by a dashed line. The power law (1) with $\xi_0 = 0.28\sigma$ is shown by a solid line. The temperature where $L_0 \approx \xi_-$ is marked by a star.

for long-range fluid–surface interactions [15] and with experimental evidences for the absence of a drying transition at subcritical temperatures even in a system with extremely weak fluid–surface interaction [3, 25], similar to the one used in our studies. Additionally, we have shown how the thickness L_0 of the drying layer can be strongly suppressed by strengthening of the fluid–surface interaction, extension of its attractive range and by confinement.

In the temperature range of our simulation studies, the correlation length ξ_- does not exceed the thickness of the drying layer L_0 (see table 1 and figure 15). However, the divergence of the correlation length ξ_- is much stronger than the logarithmic-like divergence of L_0 when approaching the critical point. Therefore, the interface between liquid and drying layer approaches the wall with increasing temperature, if the distance is measured in terms of the bulk correlation length. Assuming validity of equations (7) and (1) also closer to the critical point, the characteristic temperature, where $\xi_- \approx L_0$, can be expected at $\tau \approx 0.01$ (see star in figure 15). Above this temperature, the effective 'thickness' of the total region of density depletion near the surface should diverge asymptotically as the correlation length. This corroborates the theoretical expectations for the thickness of the wetting (drying) layer, when the critical wetting (drying) transition occurs at the bulk critical temperature [16]. Experiments with fluid mixtures indicate that the partial wetting layer decays exponentially with distance from the surface and its effective 'thickness' is proportional to the bulk correlation length ξ_- [42, 43].

We found that the total excess desorption due to the depletion of the liquid density near a weakly attractive surface should diverge as the bulk correlation length $\xi_- \sim \tau^{-\nu} = \tau^{-0.63}$ when approaching the critical temperature. This strong divergence, described by equation (9), originates from that part of the liquid density profile which extends from the bulk liquid to the inflection point of the liquid–drying layer interface. Slight variations of the fluid–surface potential do not affect noticeably this part of the profiles (see figure 12, lower panel) and, accordingly, the value of Γ_ξ, whereas the thickness of the drying layer is highly sensitive to the details of the fluid–surface potential (figure 12, upper panel).

The observed divergence of the excess desorption is stronger than $\Gamma \sim \tau^{\beta-\nu} = \tau^{-0.305}$, expected from the theory of critical adsorption [44]. We do not see the possibility of a crossover of Γ to the power law of critical adsorption with further approaching the critical temperature, as the inflection point of the liquid–drying layer interface asymptotically approaches the value $\rho_c/2$. Such a crossover could be possible only if the drying layer transforms into a vapour layer and, accordingly, the density at the inflection point of the liquid–vapour interface approaches ρ_c with increasing temperature. However, this scenario is forbidden for systems with long-range fluid–surface interaction, where vapour layers do not appear below the critical temperature [15, 16, 24]. Note that recent experimental studies of the adsorption in binary mixtures indicate that at subcritical temperatures Γ diverges more strongly than $\sim\tau^{\beta-\nu}$ [43, 45]. Such behaviour may have the same origin as that observed in our computer simulations.

Acknowledgments

References

[1] Christenson H K and Claesson P M 2001 *Adv. Colloid Interface Sci.* **91** 391
[2] Vinogradova O I 1999 *Int. J. Miner. Process* **56** 31
[3] Hess G B, Sabatini M J and Chan M H W 1997 *Phys. Rev. Lett.* **78** 1739
[4] Doerr A K, Tolan M, Seydel T and Press W 1998 *Physica* B **248** 263
    Doerr A K, Tolan M, Schlomka J-P and Press W 2000 *Europhys. Lett.* **52** 330
[5] Steitz R, Gutberlet T, Hauss T, Klosgen B, Krastev R, Schemmel S, Simonsen A C and Findenegg G H 2003 *Langmuir* **19** 2409
[6] Jensen T R, Jensen M O, Reitzel N, Balashev K, Peters G H, Kjaer K and Bjornholm T 2003 *Phys. Rev. Lett.* **90** 086101
[7] Lakshminarayanan V and Sur U K 2003 *Pramana J. Phys.* **61** 1739
[8] Schwendel D, Hayashi T, Dahint R, Pertsin A, Grunze M, Streitz R and Schreiber F 2003 *Langmuir* **19** 2284
[9] Cahn J W 1977 *J. Chem. Phys.* **66** 3667
[10] Nakanishi H and Fisher M E 1982 *Phys. Rev. Lett.* **49** 1565
[11] Pandit R, Schick M and Wortis M 1982 *Phys. Rev.* B **26** 5112
[12] Dietrich S 1988 *Phase Transitions and Critical Phenomena* vol 1, ed C Domb and J L Lebowitz (New York: Academic) p 1
[13] Binder K and Landau D P 1988 *Phys. Rev.* B **37** 1745
[14] Swol F and Henderson J R 1989 *Phys. Rev.* A **40** 2567
[15] Ebner C and Saam W F 1987 *Phys. Rev.* B **35** 1822
    Ebner C and Saam W F 1987 *Phys. Rev. Lett.* **58** 587
[16] Nightingale M P and Indekeu J O 1985 *Phys. Rev.* B **32** 3364
[17] Shahidzadeh N, Bonn D, Ragil K, Broseta D and Meunier J 1998 *Phys. Rev. Lett.* **80** 3992
[18] Henderson J R and van Swol F 1985 *Mol. Phys.* **56** 1313
[19] Evans R, Roth R and Bryk P 2003 *Europhys. Lett.* **62** 815
[20] Stewart M C and Evans R 2005 *Phys. Rev.* E **71** 011602
[21] Swol F and Henderson J R 1991 *Phys. Rev.* A **43** 2932
[22] Nijmeijer M J P, Bruin C, Bakker A F and van Leeuwen J M J 1991 *Phys. Rev.* B **44** 834
[23] Henderson J R, Tarazona P, van Swol F and Valasco E 1992 *J. Chem. Phys.* **96** 4633
[24] Nijmeijer M J P, Bruin C, Bakker A F and van Leeuwen J M J 1992 *J. Phys.: Condens. Matter* **4** 15
[25] Ancilotto F, Curtarolo S, Toigo F and Cole M W 2001 *Phys. Rev. Lett.* **87** 206103
[26] Dietrich S 2001 private communication
[27] Brovchenko I, Geiger A and Oleinikova A 2005 *Eur. Phys. J.* B **44** 345
[28] Binder K 1983 *Phase Transitions and Critical Phenomena* vol 8, ed C Domb and J L Lebowitz (London: Academic) p 1
[29] Diehl H W 1994 *Ber. Bunsenges. Phys. Chem.* **98** 466
    Diehl H W 1994 *Phys. Rev.* B **49** 2846

[30] Brovchenko I, Geiger A and Oleinikova A 2004 *J. Phys.: Condens. Matter* **16** S5345
[31] Brovchenko I and Oleinikova A 2005 *Handbook on Theoretical and Computational Nanotechnology* ed M Rieth and W Schommers (Los Angeles: American Scientific Publishers) chapter 62, at press
[32] Guida R and Zinn-Justin J 1998 *J. Phys. A: Math. Gen.* **31** 8103
[33] Panagiotopoulos A Z 1987 *Mol. Phys.* **62** 701
[34] Wilding N B 1995 *Phys. Rev.* E **52** 602
[35] Brovchenko I, Geiger A, Oleinikova A and Paschek D 2003 *Eur. Phys. J.* E **12** 69
[36] Brovchenko I, Geiger A and Oleinikova A 2004 *J. Chem. Phys.* **120** 1958
[37] van der Waals J D 1894 *Z. Phys. Chem. Stoechiom. Verwandtschaftsl.* **13** 657
[38] Fisk S and Widom B 1969 *J. Chem. Phys.* **50** 3219
[39] Buff F P, Lovett R A and Stillinger F H 1965 *Phys. Rev. Lett.* **15** 621
[40] Mecke K R and Dietrich S 1999 *Phys. Rev.* E **59** 6766
[41] Thomson W T 1871 *Phil. Mag.* E **42** 448
[42] Bonn D and Ross D 2001 *Rep. Prog. Phys.* **64** 1085
[43] Bowers J, Zarbakhsh A, Querol A, Chistenson H K, McLur I A and Cubitt R 2004 *J. Chem. Phys.* **121** 9058
[44] Fisher M E and de Gennes P G 1978 *C. R. Acad. Sci.* B **287** 207
[45] Schulz J, Bowers J and Findenegg G H 2001 *J. Phys. Chem.* B **105** 6956